

When can the Planck satellite measure spectral index running?

Cédric Pahud, Andrew R. Liddle, Pia Mukherjee, and David Parkinson

Astronomy Centre, University of Sussex, Brighton BN1 9QH, United Kingdom

10 October 2018

ABSTRACT

We use model selection forecasting to assess the ability of the Planck satellite to make a positive detection of spectral index running. We simulate Planck data for a range of assumed cosmological parameter values, and carry out a three-way Bayesian model comparison of a Harrison–Zel’dovich model, a power-law model, and a model including running. We find that Planck will be able to strongly support running only if its true value satisfies $|dn/d \ln k| > 0.02$.

Key words: cosmology: theory

1 INTRODUCTION

Results from the Wilkinson Microwave Anisotropy Probe (WMAP), especially the first-year data (Spergel et al. 2003) and to some extent the three-year data (Spergel et al. 2007), have placed a focus on possible running of the spectral index of density perturbations (see e.g. Lidsey & Tavakol 2003; Kawasaki, Yamaguchi & Yokoyama 2003; Chung, Shiu & Trodden 2003; Bastero-Gil, Freese & Mersini-Houghton 2003; Chen et al. 2004; Covi et al. 2004; Ashoorioon, Hovdebo & Mann 2005; Ballesteros, Casas & Espinosa 2006; Cline & Hoi 2006; Cortês & Liddle 2006; Easther & Peiris 2006). It is certainly premature to draw any strong conclusions based on existing evidence, especially as it remains controversial whether current data even support power-law models over the Harrison–Zel’dovich (HZ) model, but it is timely to investigate the extent to which the upcoming Planck satellite may resolve the situation.

As we have stressed in several recent papers (e.g. Mukherjee, Parkinson & Liddle 2006a; Parkinson, Mukherjee & Liddle 2006; Liddle, Mukherjee & Parkinson 2006a), the appropriate statistical tool for assessing the need to introduce new parameters is *model selection* (Jeffreys 1961; MacKay 2003; Gregory 2005). Model selection assigns probabilities to *sets* of parameters, i.e. models, in addition to the usual probability distributions for parameter values within each model. For example, Bayesian model selection applied to data compilations including WMAP3 shows that the case for including even just the spectral index n_S as a variable fit parameter is inconclusive (Parkinson et al. 2006).

In a recent paper (Pahud et al. 2006), we used model selection forecasting tools to assess the ability of the Planck satellite to distinguish between the Harrison–Zel’dovich model with $n_S = 1$ and a model with varying spectral index, VARY n . The outcome naturally depends on the assumed true value of n_S , which we call the *fiducial value*, and we found that Planck can strongly favour the latter model only if the true value of n_S lies outside the range $[0.986, 1.014]$. In making that comparison, we assumed that the true spectrum could be described by a power-law.

In this paper, we extend that analysis to include the possibility of spectral index running, given by $\alpha \equiv dn/d \ln k$. This adds an extra model, VARY $n\alpha$, to the model set. This means that we are carrying out a three-way model comparison, within the two-dimensional space defined by the fiducial values of n_S and α . Ideally we would also have included tensor perturbations in this analysis in order to fully represent the usual inflationary predictions (e.g. Liddle & Lyth 2000), but the present analysis is at the limits of current computer power, having required many months of multi-processor time.

2 MODEL SELECTION FORECASTS FOR MODELS WITH RUNNING

2.1 Model selection forecasting

Our approach exactly follows our earlier paper (Pahud et al. 2006), and so we provide only the briefest of summaries here and refer to that paper and references therein for details. Model selection forecasting was first introduced by Trotta (2007b), whose Predictive Posterior Odds Distribution (PPOD) forecasting determined the probability of different model selection outcomes of future experiments based on present knowledge. An alternative approach, which delineates regions of parameter space where different model selection verdicts are expected, was introduced in Mukherjee et al. (2006b); a combination of the methods was used in Pahud et al. (2006), and also subsequently in Trotta (2006), Liddle et al. (2006b) and Trotta (2007a). As used here, data are simulated for the different possible true values of the parameters of interest, known as fiducial values, and a model comparison analysis carried out at each point.

Although not required, in typical examples a simple model will be nested within a more complex one, e.g. the HZ model is the special case of VARY n with $n_S = 1$. If the (assumed) true model is the nested one, the model comparison will favour that model, and one may ask how strongly. If instead the true model is the more complex one, one can ask how far from the simple model the true

arXiv:astro-ph/0701481v2 4 Sep 2007

values would have to be, in order that a given experiment can overcome statistical uncertainty and deliver a strong or decisive verdict in favour of the complex model. These two notions can be used to define model selection Figures-of-Merit, assessing the abilities of competing experiments (Mukherjee et al. 2006b).

In our work, we use the Bayesian evidence E as the model selection statistic. Like any model selection statistic, it creates a tension between goodness of fit to the data and the complexity of the model. It represents a full implementation of Bayesian inference, being the probability of the data given the model (i.e. the model likelihood). It updates the prior model probability to the posterior model probability. Computations are carried out using the nested sampling algorithm (Skilling 2006), using our code COSMONEST¹ (Mukherjee et al. 2006a; Parkinson et al. 2006). Computing the evidence accurately is significantly more challenging than computing the posterior probability distribution, and so the calculations are computationally time-consuming.

Our assumption is that there are three models of interest in fitting future Planck data. These are the Harrison–Zel’dovich model, a power-law model where n_S is fit from data, and a model where both n_S and α are varied. We denote these models HZ, VARY n , and VARY $n\alpha$ respectively, and also indicate them by use of subscripts 0, 1, and 2 respectively.

In the presence of running, the spectral index is defined in the usual way by

$$n_S(k) = n_S(k_0) + \alpha \ln \frac{k}{k_0}. \quad (1)$$

The pivot scale $k_0 = 0.05 \text{ Mpc}^{-1}$ corresponds to a scale well constrained by existing data. When running is included, n_S is always specified at this scale, and throughout we assume the running is constant. As in Pahud et al. (2006), the prior range for n_S is taken to be $0.8 < n_S < 1.2$, representing a reasonable range allowed by slow-roll inflation models (see e.g. Liddle & Lyth 2000).

We take the prior on α to be $-0.1 < \alpha < 0.1$. This is somewhat arbitrary. Slow-roll inflation models would tend to suggest a much smaller value (Kosowsky & Turner 1995), but there is no point in restricting the analysis to values smaller than Planck can measure, as one will simply conclude that Planck is unable to make the measurement. Accordingly, our range is loosely motivated by present observational knowledge, corresponding to models with unexpectedly large running. The comparison between two models does have some prior dependence on the extra parameter(s). If one prior is widened in regions where the likelihood is negligible, then the evidence changes proportional to the prior volume, so for instance a doubling of the prior range will only reduce $\ln E$ by $\ln 2 = 0.69$.

In running CosmoNest, the algorithm parameters used were $N = 300$ live points and an enlargement factor of 1.8 for HZ, 1.9 for VARY n , and 2.0 for VARY $n\alpha$. The tolerance parameter was set to 20 (rather than 0.5 as in our previous analysis) in order to improve the speed of the simulations. This is sufficient to give answers to good accuracy as indicated by the uncertainties obtained. Four independent evidence evaluations were done for each calculation, to obtain the mean and its standard error.

We then compare our models in pairs by considering the Bayes factor, defined as the ratio of evidences between two models, written $B_{ij} = E(M_i)/E(M_j)$, for $i, j = 0, 1, 2$ ($i \neq j$), where M_i and M_j indicate the two models under assumption. By plot-

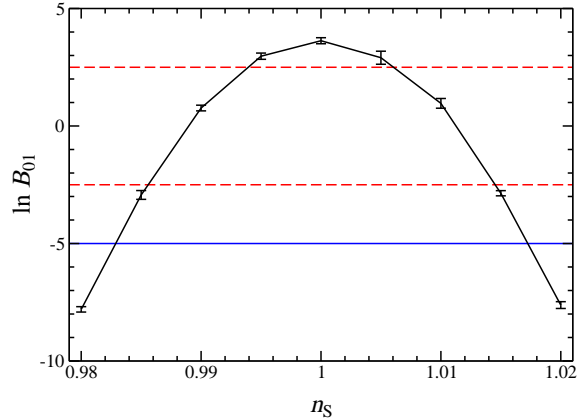


Figure 1. The logarithm of the Bayes factor, $\ln B_{01}$, as a function of the fiducial value of n_S . The horizontal lines indicate where the comparison becomes ‘strong’ (dashed) and ‘decisive’ (solid) on the Jeffreys’ scale.

ting the Bayes factor using datasets generated as a function of the two parameters of interest, one uncovers the regions of the two-dimensional fiducial parameter space in which the Planck satellite would be able to decisively select between the two models, and also those regions where the comparison would be inconclusive.

In order to assess the significance of any difference in evidence between two models, a useful guide is given by the Jeffreys’ scale (Jeffreys 1961). Labelling as M_i the model with the higher evidence, it rates $\ln B_{ij} < 1$ as ‘not worth more than a bare mention’, $1 < \ln B_{ij} < 2.5$ as ‘substantial’, $2.5 < \ln B_{ij} < 5$ ‘strong’ to ‘very strong’, and $5 < \ln B_{ij}$ as ‘decisive’.

2.2 Simulating Planck data

We simulate Planck data exactly as described in Pahud et al. (2006). Having determined the fiducial model power spectra, we simulate temperature power spectrum data for the three most sensitive High Frequency Instrument (HFI) channels and the polarization signal for only one of these channels, modelling instrument noise using current detector specifications. The simulations are somewhat simplistic, as computational limitations prevent a more detailed treatment that might include residuals from foreground subtraction and $1/f$ noise. However they should provide a good characterization of the Planck data for our purposes. Simulations are carried out for various values of the spectral index and its running, and the other parameters are those of the usual Λ CDM model in a flat spatial geometry.

In simulating the data, we are primarily interested in the dependence on the key parameters of interest, n_S and α , and different data simulations are carried out for a grid of values in that plane. The other cosmological parameters are given fixed fiducial values as in Pahud et al. (2006), namely the baryon physical density $\Omega_b h^2 = 0.024$, the cold dark matter physical density $\Omega_c h^2 = 0.103$, the sound horizon $\Theta = 1.047$, the optical depth $\tau = 0.14$, and the density perturbation amplitude normalization $A_S = 2.3 \times 10^{-9}$. The corresponding value of the Hubble parameter is $h = 0.78$. The model selection verdict should have negligible dependence on these fiducial values. Note that all parameters, including these, are varied in computing the evidences of the models; it is only in defining the fiducial models for data simulation that these parameters are fixed. The prior ranges used for these parameters are as in Pahud et al. (2006): $0.018 \leq \Omega_b h^2 \leq 0.032$,

¹ Available at <http://cosmonest.org>.

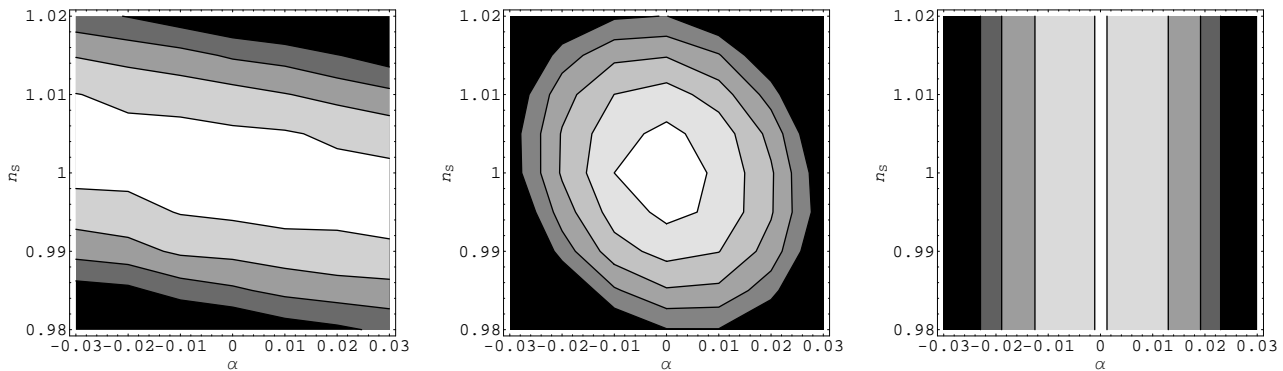


Figure 2. The logarithm of the Bayes factors, $\ln B_{01}$ in the left panel, $\ln B_{02}$ in the centre, and $\ln B_{12}$ in the right, as a function of the fiducial values of n_s and α . The contour lines represent different steps in the Jeffreys’ scale. From the plot centres, the levels are 2.5, 0, -2.5, -5 in the left and right panels, with the centre panel contours starting at 5.

$$0.04 \leq \Omega_c h^2 \leq 0.16, 0.98 \leq \Theta \leq 1.1, 0 \leq \tau \leq 0.5, \text{ and } 2.6 \leq \ln(A_S \times 10^{10}) \leq 4.2.$$

3 RESULTS

We begin by showing in Fig. 1 the main result obtained in Pahud et al. (2006). In that analysis, running was not included and so the fiducial α is zero. At $n_s = 1$, corresponding to HZ being the true model, the HZ model is strongly preferred with $\ln B_{01} = 3.6 \pm 0.1$. It has a higher evidence since it can fit the data just as well as VARY n and has one less parameter. Once n_s is far enough away from 1, the HZ fit becomes very poor and the Bayes factor plummets. The speed with which this happens indicates the strength of the experiment. The VARY n model becomes strongly favoured only once $n_s < 0.986$ or $n_s > 1.014$; if the true value lies within that range even the Planck satellite will give inconclusive results.

Figure 2 shows the extension of our results into the α - n_s plane, now showing the three-way model comparison. The left plot still shows the comparison between HZ and VARY n , though neither is the true model except at $\alpha = 0$ (Fig. 1 is the cross-section of this plot at $\alpha = 0$). The plot is not surprising in the sense that the logarithm of the Bayes factor is roughly independent of α . The models HZ and VARY n are just as bad at describing a non-zero running. However, a slight tilt of the contours appears when α goes away from zero. This indicates that a positive (resp. negative) running can be balanced by a scalar index smaller (resp. bigger) than 1, accordingly to equation (1). This can benefit HZ or VARY n , depending whether it helps or hinders the HZ model to fit the data. In fact the effect just reflects that the scale k_0 is not quite at the statistical centre of the data, so that the determination of n_s and α has some correlations, and could be removed by judicious choice of the ‘pivot’ scale (Cortés, Liddle & Mukherjee 2007).

The centre panel now introduces a comparison of HZ with VARY $n\alpha$, which is the true model in most of the parameter plane. At $[\alpha, n_s] = [0, 1]$, the HZ model is decisively preferred with $\ln B_{02} = 6.3 \pm 0.1$. Its higher evidence arises since it can fit the data just as well as VARY $n\alpha$, but has two less parameters. Once the fiducial point in the two-dimensional space is far enough away from the centre, the HZ fit becomes very poor and VARY $n\alpha$ model becomes favoured.

Being the true model, VARY $n\alpha$ can simply adapt its two extra free parameters to fit the data at every point of the fiducial space

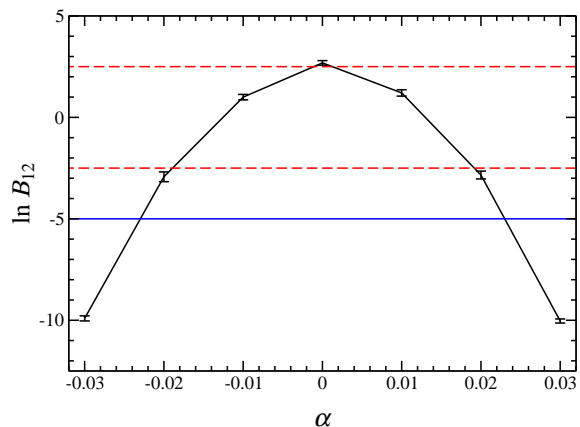


Figure 3. The logarithm of the Bayes factor, $\ln B_{12}$, as a function of the fiducial value of α . The horizontal lines indicate where the comparison becomes ‘strong’ (dashed) and ‘decisive’ (solid) on the Jeffreys’ scale.

equivalently, thus leading to the same evidence. We have verified this holds to excellent accuracy in our simulations. The behaviour of the Bayes factor should therefore be approximately symmetrical with respect to $n_s = 1$ and to $\alpha = 0$. However, it is clearly not quite the case, for the same reason as the presence of the tilt in the left panel. The influence of the correlation between the two fiducial parameters is greater this time, as it acts on HZ only.

Finally, we need to consider a comparison between the models VARY n and VARY $n\alpha$, which is illustrated in the right panel of Fig. 2. This plot is fully determined by the above results, as by definition $\ln B_{12} = \ln B_{02} - \ln B_{01}$. Moreover, for the same reason that the evidence of VARY $n\alpha$ is independent of both fiducial parameters n_s and α , VARY n turns out to be independent of n_s . This allows us to restrict our analysis to one dimension only, shown in Fig. 3. At $\alpha = 0$ the VARY n model is strongly preferred over VARY $n\alpha$ as $\ln B_{12} = 2.7 \pm 0.1$, having one less parameter. The running model becomes strongly favoured only if the true running satisfies $|\alpha| > 0.02$.

In Fig. 4, we display the full three-way model comparison in two different ways. The three-model case is perfectly adapted to display by false-colour RGB plot, where the intensity of each of the three red–green–blue colour channels at a given fiducial point

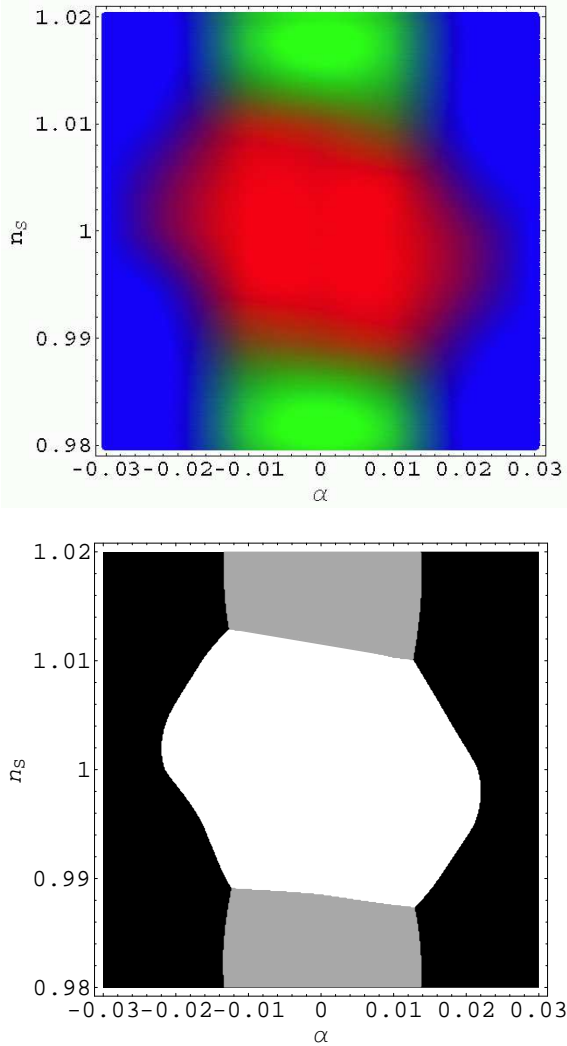


Figure 4. Two graphical representations of the three-way model comparison. The upper panel is a false-colour RGB plot with the probabilities of HZ, VARY n , and VARY $n\alpha$ assigned to the red, green, and blue channels respectively. The lower panel simply shows the model which would receive the highest model probability at each point in the fiducial parameter space, with those three models allocated white, grey, and black respectively.

is assigned as the posterior model probability, given by Bayes’ theorem,

$$P_i = P(M_i|D) = \frac{P(D|M_i)P(M_i)}{\sum_j P(D|M_j)P(M_j)}. \quad (2)$$

Here we assume that the prior model probabilities $P(M_i)$ are equal (an assumption readily varied if required), so the equation simplifies to

$$P_i = \frac{E(M_i)}{\sum_j E(M_j)}. \quad (3)$$

That the total probability sums to one corresponds to fixed total intensity. This is shown in the upper panel. The region which appears red would lead to the HZ model being preferred, green the VARY n model, and blue the VARY $n\alpha$ model. Between those, regions which interpolate into secondary colours share their probability between the different models. There are also four ‘vertices’

at which all three models have the same probability. We see that the transitions between the different domains are rather rapid in terms of the shifting model probabilities.

The lower plot shows a much simpler representation, where regions are shaded simply according to the dominant model probability in that region.

These two plots affirm the results already apparent from the earlier figures; for Planck to be able to demonstrate that $n_S \neq 1$, the true value will have to be more than 0.01 away from unity (Pahud et al. 2006), and for running to be convincingly detected $|\alpha|$ will need to be at least 0.02.

4 CONCLUSIONS

According to WMAP3 analyses (Spergel et al. 2007), the running is presently constrained, at 95% confidence, to be in the range of approximately $-0.17 < \alpha < +0.01$. The precise constraints depend on both on the dataset combination used and the model assumptions made (e.g. whether or not to include tensor perturbations), and we have simply quoted the broadest available. Although the range is highly skewed to negative values, the special status of $\alpha = 0$, and the prediction from slow-roll inflation for an α value that current experiments cannot distinguish from zero, means that from a model selection point of view $\alpha = 0$ should still be regarded as a very plausible interpretation of the data.

Given this inconclusive position, we have addressed the extent to which the Planck satellite is likely to resolve the situation, using model selection tools to compare three models: Harrison-Zel’dovich (HZ), power-law initial perturbations (VARY n), and the running model (VARY $n\alpha$). The expected outcome depends, of course, on which (if any) of these models proves to be the correct one.

Supposing first that HZ is the true model, we found in Pahud et al. (2006) that VARY n would be strongly, though not decisively, disfavoured after Planck. The present paper adds the new information that the running model would be decisively disfavoured in this circumstance.

Suppose instead that VARY n is true. Then VARY n will be strongly, but not decisively, preferred over VARY $n\alpha$. However, as shown in Pahud et al. (2006), the true value of n_S has to be sufficiently far from one in order for VARY n to be favoured over HZ. Depending on the true parameter values, all three models may survive application of Planck data.

Finally, suppose VARY $n\alpha$ is true. The alternatives will only be decisively ruled out provided the true value satisfies $|\alpha| \gtrsim 0.02$, otherwise the outcome will again be indecisive. The conclusion is that Planck will improve knowledge as compared to WMAP3, by a factor of around four (our calculations indicate a projected parameter uncertainty from Planck of about ± 0.007 on α , to be compared with the current ± 0.03 from WMAP3 alone), and thus does have the capability to convincingly detect running if it is prominent. However, it does not have the accuracy to probe into the region where slow-roll inflation models typically lie (Kosowsky & Turner 1995).

Our analysis refers to Planck satellite data alone, and, as with WMAP3, one would expect some further tightening with incorporation of other datasets probing different length scales.

As with any Bayesian analysis, the results have some dependence on prior assumptions. For the priors we have chosen on n_S and α , the data are able to constrain the likelihood well within them. Consequently, any change in prior ranges that continues to respect

this will just change the evidences according to the change in volume, an effect one can readily calculate. Bearing in mind that the Jeffreys' scale is logarithmic, a sizeable change in prior parameter ranges would be needed to significantly alter the conclusions.

ACKNOWLEDGMENTS

C.P. was supported in part by the Swiss Sunburst Fund, and A.R.L., P.M., and D.P. by PPARC. C.P. acknowledges the hospitality of Caltech and Marc Kamionkowski while this work was completed, during a visit supported by the Royal Astronomical Society and by Caltech. A.R.L. acknowledges the hospitality of the Institute for Astronomy, University of Hawai'i, while this work was being completed. We thank Jim Cline for prompting us to look at this issue.

REFERENCES

- Ashoorioon A., Hovdebo J. L., Mann R. B., 2005, Nucl. Phys. B, 727, 63, gr-qc/0504135
- Ballesteros G., Casas J. A., Espinosa J. R., 2006, JCAP, 0603, 001, hep-ph/0601134
- Bastero-Gil M., Freese K., Mersini-Houghton L., 2003, Phys. Rev. D, 68, 123514, hep-ph/0306289
- Chen. C., Feng B., Wang X., Yang Z., 2004, Class. Quant. Grav., 21, 3223, astro-ph/0404419
- Chung D. J. H., Shiu G., Trodden M., 2003, Phys. Rev. D, 68, 063501, astro-ph/0305193
- Cline J. M., Hoi L., 2006, JCAP, 0606, 007, astro-ph/0603403
- Cortés M., Liddle A. R., 2006, Phys. Rev. D, 73, 083523, astro-ph/0603016
- Cortés M., Liddle A. R., Mukherjee P., 2007, Phys. Rev. D, 75, 083520, astro-ph/0702170
- Covi L., Lyth D. H., Melchiorri A., Odman C. J., 2004, Phys. Rev. D, 70, 123521, astro-ph/0408129
- Easther R., Peiris H., 2006, JCAP, 0609, 010, astro-ph/0604214
- Gregory P., 2005, *Bayesian logical data analysis for the physical sciences*, Cambridge University Press
- Jeffreys H., 1961, *Theory of Probability*, 3rd ed, Oxford University Press
- Kawasaki M., Yamaguchi M., Yokoyama J., 2003, Phys. Rev. D, 68, 023508, hep-ph/0304161
- Kosowsky A., Turner M. S., 1995, Phys. Rev. D, 52, 1739, astro-ph/9504071
- Liddle A. R., Lyth D. H., 2000, *Cosmological inflation and large-scale structure*, Cambridge University Press
- Liddle A. R., Mukherjee P., Parkinson D., 2006a, A&G, 47, 4.30, astro-ph/0608184
- Liddle A. R., Mukherjee P., Parkinson D., Wang Y., 2006b, Phys. Rev. D, 74, 123506, astro-ph/0610126
- Lidsey J. E., Tavakol R., 2003, Phys. Lett. B, 575, 157, astro-ph/0304113
- MacKay D. J. C., 2003, *Information theory, inference and learning algorithms*, Cambridge University Press
- Mukherjee P., Parkinson D., Liddle A. R., 2006a, ApJL, 638, L51, astro-ph/0508461
- Mukherjee P., Parkinson D., Corasaniti P. S., Liddle A. R., Kunz M., 2006b, MNRAS, 369, 1725, astro-ph/0512484
- Pahud C., Liddle A. R., Mukherjee P., Parkinson D., 2006, Phys. Rev. D, 73, 123524, astro-ph/0605004
- Parkinson D., Mukherjee P., Liddle A. R., 2006, Phys. Rev. D, 73, 123523, astro-ph/0605003
- Skilling J., 2006, Bayesian Anal., 1, 833
- Spergel D. N. et al. (the WMAP Team), 2003, ApJS, 148, 175, astro-ph/0302209
- Spergel D. N. et al. (the WMAP Team), 2007, ApJS, 170, 377, astro-ph/0603449
- Trotta R., 2006, in proceedings of "Cosmology, galaxy formation and astroparticle physics on the pathway to the SKA", astro-ph/0607496

- Trotta R., 2007a, MNRAS, 378, 72, astro-ph/0504022
- Trotta R., 2007b, MNRAS, 378, 819, astro-ph/0703063

This paper has been typeset from a $\text{\TeX}/\text{\LaTeX}$ file prepared by the author.